

Three-Dimensional Orientation of Compact High Velocity Clouds

F. Heitsch,^{1*} B. Bartell,¹ S.E. Clark,^{1,2} J.E.G. Peek,^{2,3} D. Cheng¹ and M. Putman²

¹*Department of Physics and Astronomy, University of North Carolina Chapel Hill, Chapel Hill, NC 27599-3255, U.S.A*

²*Department of Astronomy, Columbia University, 550 W 120th St, New York, NY 10027, U.S.A*

³*Space Telescope Science Institute, 3700 San Martin Dr, Baltimore, MD 21218, U.S.A*

Accepted 2016 June 21 Received 2016 June 21; in original form 2016 March 24

ABSTRACT

We present a proof-of-concept study of a method to estimate the inclination angle of compact high velocity clouds (CHVCs), i.e. the angle between a CHVC’s trajectory and the line-of-sight. The inclination angle is derived from the CHVC’s morphology and kinematics. We calibrate the method with numerical simulations, and we apply it to a sample of CHVCs drawn from HIPASS. Implications for CHVC distances are discussed.

Key words: Galaxy:halo — Galaxy:evolution — hydrodynamics — turbulence — methods:numerical — methods:observational

1 MOTIVATION

The Galactic halo hosts a population of neutral hydrogen clouds whose line-of-sight velocities are inconsistent with Galactic rotation (Wakker & van Woerden 1997). These High Velocity Clouds (HVCs) range from large “complexes” of many degrees to structures at the resolution limit. Their diversity suggests different origins (Wakker & van Woerden 1997; Putman et al. 2012). Distances to HVCs are key to the origin question. The most accurate constraints stem from absorption line studies (Wakker 2001; Wakker et al. 2007; Thom et al. 2006, 2008; Richter et al. 2015), yet these are only available for structures of large angular extent, and therefore are biased to near objects. Indirect distances via H α emission use the UV flux escaping from the disk and ionizing the HVCs (Putman et al. 2003). Uncertainties arise from determining the escape fraction of ionizing UV photons, though the patchiness of the disk interstellar gas ceases to be of concern for $|z| > 10$ kpc (Bland-Hawthorn & Putman 2001; Peek et al. 2007). Olano (2008) uses a putative origin to constrain distances of CHVCs spatially associated with the Magellanic complexes (also Peek et al. 2008; Saul et al. 2012). Distance constraints based on cloud kinematics assume a terminal velocity for HVCs (Benjamin & Danly 1997) or rely on differential drag due to the interaction with the background medium (Peek et al. 2007). Both of these methods require the inclination angle between the cloud’s trajectory and the line-of-sight. Full trajectory information has been inferred in only

a few cases (Smith Cloud: Lockman et al. 2008; Fox et al. 2016; Complex GCN: Jin 2010).

We will focus our attention on compact high velocity clouds (CHVCs), many of whom show a head-tail structure, consisting of a cold, dense core, and a more diffuse, warmer tail (Brüns et al. 2000, 2001). This morphology suggests that CHVCs interact with the ambient medium during their passage through the Galactic halo (Brüns et al. 2000; Stanimirović et al. 2006; Peek et al. 2007; Putman et al. 2011). Because of their small angular extent, distance estimates to CHVCs stem mostly from assumed association with larger complexes (Peek et al. 2008; Putman et al. 2011). Yet, an independent method is desirable. Because of their interaction with the ambient gas, CHVCs could in principle be used to gain information about the elusive gaseous component of the Galactic halo (Peek et al. 2007).

Instead of aiming directly at getting distances to CHVCs, we propose a method to determine the three-dimensional orientation of CHVCs and thus their full, three-dimensional velocity \mathbf{v}_{tot} . Consequences for distance constraints are discussed in Sec. 4.1.

2 THE METHOD

The coordinate system is set by the local (GL, GB) patch describing the plane-of-sky, and by the (unknown) cloud distance D along the line-of-sight (Fig. 1). The three-dimensional orientation of a CHVC requires two angles: The inclination angle $0 \leq \alpha_i \leq \pi$ describes the angle between the cloud *tail* and the line-of-sight, with the tail pointing away from the observer for $\alpha_i = 0$. The position angle

* E-mail: fheitsch@unc.edu

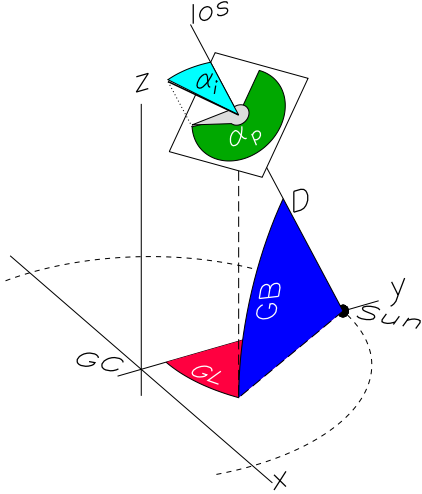


Figure 1. Definition of the coordinate system for CHVC orientation. The position angle α_p (green) and the inclination angle α_i (cyan) are defined in the local (GL,GB) patch, at an (unknown) distance D from the Sun. A cartoon CHVC mapped within the local (GL,GB) patch is outlined in grey.

$0 \leq \alpha_p < 2\pi$ is counted counter-clockwise starting with $\alpha_p = 0$ for the cloud's tail pointing toward Galactic North. The local coordinate patch is assumed to be rectangular – hence the limitation to CHVCs.

The goal is to relate the cloud shape in position-velocity space to the inclination angle. We demonstrate the process with the help of a simulation (Fig. 2) of a CHVC traveling at $\alpha_i = 45^\circ$ toward the observer. The simulation (model Wb1a15b of Heitsch & Putman (2009), see their table 1 and fig. 2) is a wind-tunnel experiment, in which an initially spherical cloud of (in this case) radius 50 pc and density 0.1 cm^{-3} is exposed to a wind of 150 km s^{-1} and a density of 10^{-5} cm^{-3} . The simulation generated ~ 30 3D data sets consisting of gas density, velocity and temperature. These are converted into position-position-velocity cubes by selecting for gas with a temperature of $T < 10^4 \text{ K}$ (assumed to be neutral hydrogen), rotating by the desired inclination angle α_{i0} , and then calculating channel maps with $\Delta v = 1 \text{ km s}^{-1}$ assuming optically thin HI-21 cm emission. Peak column densities reach $\sim 3 \times 10^{19} \text{ cm}^{-2}$. These channel maps are then used for further analysis.

The position angle α_p is determined by fitting ellipses to the integrated intensity maps. Since the orientation of the ellipse is degenerate with π , we identify the tail of the cloud as the direction in which the cloud extends farthest from the column density peak (i.e. the location of the head). This assumes that the clouds have a head-tail structure. To estimate the inclination angle, we define the cloud's "backbone" (i.e. the line through the cloud's center-of-mass at the determined α_p), along which spectra are taken to construct a position-velocity map (Fig. 2e-g). For a CHVC moving toward the observer, the (dense) core will appear at more negative velocities and the tail at more positive ones, hence the CHVC will be asymmetric along the velocity axis. Yet, along the position axis, the CHVC will appear more or less symmetric (Fig. 2d). If the CHVC moves perpendicularly to the line-of-sight, head and tail can be clearly identified,

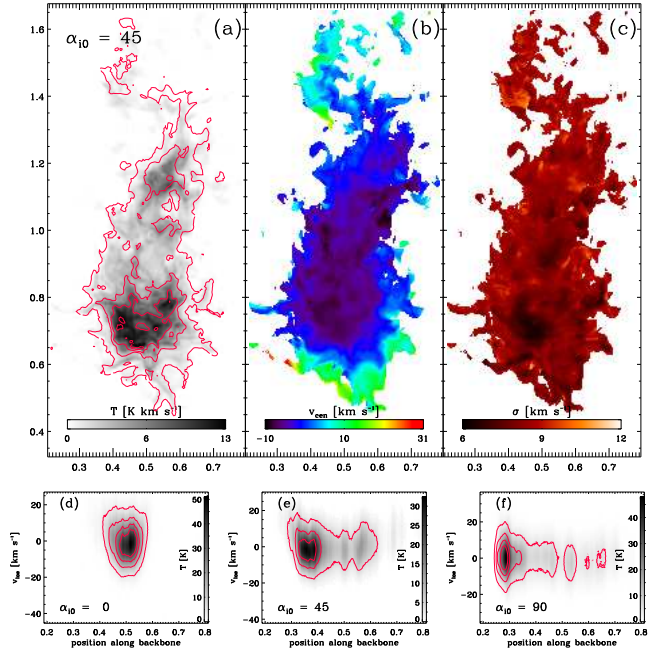


Figure 2. (a) Integrated intensity, (b) centroid velocity, and (c) velocity dispersion of a model CHVC (model Wb1a15b of Heitsch & Putman (2009)), traveling at 45° to the observer. Contours are given at $[1, 5, 9, 13] \text{ K km s}^{-1}$. (d,e,f) Position-velocity plots for inclination angles $\alpha_{i0} = 0, 45, 90^\circ$. Contours correspond to $[5, 15, 25, 35] \text{ K}$.

resulting in an asymmetry in position. Yet, the CHVC will appear symmetric in velocity space, since the gradient along the cloud backbone due to the differential drag will not be discernible, and only thermal and turbulent motions within the CHVC will contribute to the velocity signature (Fig. 2f). A CHVC traveling at e.g. 45° to the observer will appear asymmetric both in position and velocity (Fig. 2e).

We calculate the observable asymmetry of the CHVC's gas distribution with respect to its center-of-mass. The asymmetry in position is given by

$$a_p \equiv \frac{\Delta_{2p} - \Delta_{1p}}{\Delta_{1p} + \Delta_{2p}}, \quad (1)$$

with $-1 \leq a_p \leq 1$. The one-sided dispersions $\Delta_{1p,2p}$ refer to the CHVC extent to lower/higher values in position with respect to the center-of-mass, e.g.

$$\Delta_{1p} = \left(\sum_{p < p_c, v} (p - p_c)^2 T(p, v) / \sum_{p < p_c, v} T(p, v) \right)^{1/2}, \quad (2)$$

where $T(p, v)$ is the position-velocity map, p_c is the center-of-mass position, and the summation extends over all $p < p_c$ (along the horizontal axis in Fig. 2d-f), and over the whole velocity range. For Δ_{2p} , the summation extends over $p > p_c$. The velocity extents $\Delta_{1v,2v}$ are constructed similarly, along the vertical (velocity) axis of the position-velocity plot. Other measures of cloud extent, such as 50% contours, give similar results. Since the accuracy of $\Delta_{1,2}$ depends on the map resolution, spatial and velocity resolution of the telescope will affect the result. A CHVC with the tail pointing toward positive p has $a_p > 0$, and a CHVC moving toward the observer (tail toward positive v) has $a_v > 0$. Since the

asymmetries are normalized, and if we assume (to first order) a linear relationship between the velocity and the position along the cloud’s tail (see e.g. Brüns et al. 2001), we can calculate the inclination angle as

$$\alpha_i = \arctan\left(\frac{a_p}{a_v}\right). \quad (3)$$

To test the method, position-position-velocity cubes are generated for the CHVC model of Fig. 2, for a series of rotation angles α_{i0} . “Spectra” (position-velocity plots) are taken along the long axis of the cloud (Fig. 2d-f), from which we derive the inclination angle estimate α_i . Fig. 3 summarizes the reliability of the inclination angle estimates. Panels (a) and (b) show α_i as derived from equation 3, and its residuals $\alpha_i - \alpha_{i0}$. Apart from occasional large deviations due to substantial fractions of gas being stripped off the CHVC, the residuals depend systematically on the model rotation angle α_{i0} (Fig. 3f). Therefore, we attempt to improve on equation 3 by fitting a heuristic function to the residuals; we average over the cloud evolution time (Fig. 3g, the error bars are errors on the mean). The resulting corrected values are shown in red in Fig. 3e through 3g, and Fig. 3b,d. The fitting function is given by

$$f(\alpha_{i0}) = p_0 \tanh \frac{\alpha_{i0} - p_2}{p_3} \exp \frac{\alpha_{i0} - p_2}{p_4} + p_1. \quad (4)$$

Parameter distributions and values derived from the Metropolis-Hastings algorithm used to fit equation 4 are given in the right column of Fig. 3.

3 APPLICATION TO CHVCS

We apply the inclination angle estimate to selected CHVCs drawn from HIPASS (Putman et al. 2002). We select with a slight preference for head-tail clouds, yet we note that the head-tail structure would not show when the CHVC is traveling along the line-of-sight. The top two rows of Fig. 4 show the integrated intensity and centroid velocity. HIPASS catalogue numbers are given in each panel. We apply a selection ellipse around the CHVC structure of interest, removing unassociated emission, both in (GL, GB) -space and in v_{lsr} -space.

We determine the angles α_p and α_i for a sequence of increasing signal-to-noise values ($S/N = [5, 40]$ in steps of 1). For $S/N < 5$, angle estimates were generally unreliable in our sample. The bottom row of Fig. 4 summarises the derived angles for the selected CHVCs. Shown are the median values (solid lines) including lower and upper quartiles (dashed lines), to highlight the uncertainties in the angle estimates. The position angle α_p can be determined within $< \pm 3^\circ$ (exception: cloud 1804, whose position angle “drifts” with S/N). For well-defined clouds, the inclination angles show similar ranges. To further assess the reliability of the angle estimates, we calculate α_i for all $0 \leq \alpha_p \leq 360$ and for all S/N . In the resulting map of $\alpha_i(\alpha_p, S/N)$ we search for “consistent” α_i values, i.e. for regions in $(\alpha_p, S/N)$ space across which α_i does not change by more than 2° . These regions are usually extended over a large range in S/N , while for inconsistent solutions, α_i varies strongly with α_p . The largest of these regions is taken as the solution. The resulting angle estimates are consistent with the direct fits described above.

4 DISCUSSION

4.1 A Method to Constrain CHVC Distances

We explore whether the full cloud orientation can be used to derive distance constraints of CHVCs via the velocity of a CHVC relative to its background medium, v_{rel} . This requires several assumptions. It is not our intent that these be necessarily correct, but that they are sufficiently plausible to outline the method. The goal is to calculate $v_{rel} = |\mathbf{v}_{tot} - \mathbf{\Theta}|$ along the line-of-sight at a given (GL, GB) for a range of distances D . Here, \mathbf{v}_{tot} is the three-dimensional velocity of the CHVC in Galactic cartesian coordinates, and $\mathbf{\Theta}$ is the three-dimensional (halo) rotation velocity of the background medium. All velocities are relative to the Galactic Standard of Rest (GSR). Since \mathbf{v}_{tot} is constant along the line-of-sight, but $\mathbf{\Theta}$ will change with D , $v_{rel} = v_{rel}(D)$. If we have additional information on v_{rel} , such as a terminal velocity v_{max} at which CHVCs can move with respect to the background medium, distances D can be identified for which $v_{rel} \leq v_{max}$.

Setting $\mathbf{\Theta}$ requires a Galactic halo rotation model. For demonstration, we combine the rotation curve model of Fich et al. (1989) with an exponential drop-off in z , reproducing the linear gradient of -22 km s^{-1} derived by Levine et al. (2008). Our halo rotation model then reads as

$$|\mathbf{\Theta}| \equiv v_R(R_{xy}, z) = (109 + 108 R_{xy}^{0.0042}) e^{-|z|/10}, \quad (5)$$

with R_{xy} and z in kpc. The radius R_{xy} gives the Galactocentric distance in the plane, with the full Galactocentric radius being $R = (R_{xy}^2 + z^2)^{1/2}$.

There are several options to constrain v_{rel} , such as setting v_{max} to the terminal velocity due to hydrodynamical drag (Benjamin & Danly 1997), estimating v_{rel} based on differential drag analysis of the CHVC (Peek et al. 2007), or limiting v_{max} to the sound speed of the background medium for sufficiently diffuse CHVCs. Based on our models (Heitsch & Putman 2009), we choose the latter and set $v_{max} = c_s = 100 \text{ km s}^{-1}$. Other options will be explored in a future contribution.

Table 1 summarises the estimated parameters for the seven CHVCs shown in Fig. 4 together with a few other CHVCs selected from HIPASS. Roughly 50% of the sample CHVCs have near distance constraints (at $c_s = 100 \text{ km s}^{-1}$). Most remaining CHVCs show relative velocities $v_{rel} > 200 \text{ km s}^{-1}$, and thus do not lead to a distance constraint. The value of $|\mathbf{v}_{tot}|$ depends strongly on α_i : At $\alpha_i = 90, 270^\circ$, $|\mathbf{v}_{tot}|$ cannot be reconstructed.

Though none of the observed CHVCs have (previous) direct distance constraints, many of them are potentially related to larger HVC complexes with constraints from their position-velocity proximity (Peek et al. 2008; Putman et al. 2011). In the Southern sky, the majority of the HVCs (and the CHVCs in Table 1) can be associated with the Magellanic System and though the distance to the Magellanic complexes are unknown, the Magellanic Clouds themselves are at 50-60 kpc and the associated clouds are expected to be further away than the lower distance limits D_{lo} in Table 1. One strong comparison point in our sample is cloud 238, which is in the position-velocity vicinity of the tail of Complex C. Complex C has a direct distance constraint of 10 kpc (Thom et al. 2008), and we find this cloud has a lower distance estimate of 10 kpc. Within the uncertainties,

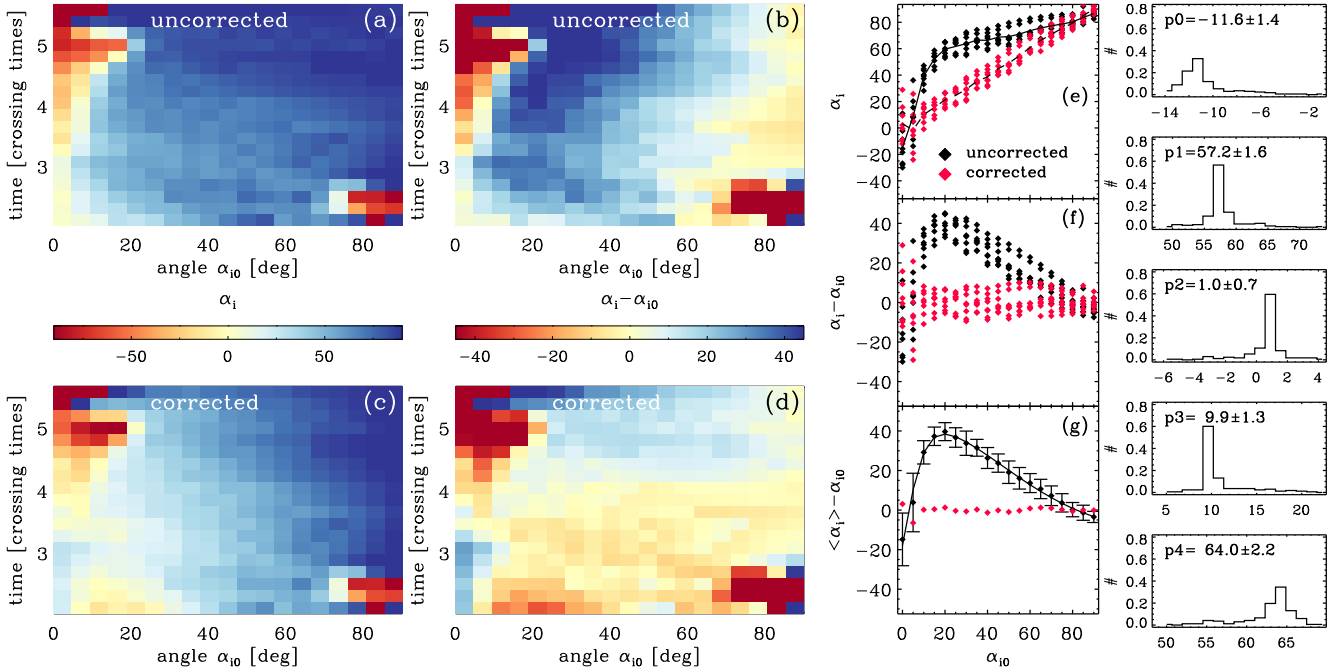


Figure 3. (a) Colour map of the uncorrected inclination angle estimate (equation 3) depending on the rotation angle α_{i0} , and on the model CHVC evolution time. Large “secular” differences occur when substantial fragments are stripped off the CHVC. (b) Uncorrected inclination angle residuals scaled between $\pm 45^\circ$. (c) Corrected inclination angle estimates, and (d) corrected residuals. (e) Uncorrected (black) and corrected (red) inclination angles, and (f) their residuals. (g) Residuals calculated from averaged uncorrected inclination angle (black), empirical fit (line, see equation 4), and resulting corrected residuals (red). The right column gives the fit parameter distributions and values.

Table 1. Selected HIPASS CHVC parameters. [1] HIPASS number. [2] Galactic longitude GL. [3] Galactic latitude GB. [4] Position angle α_p . [5] Inclination angle α_i . [6] Lower distance limit D_{lo} . [7] Total velocity $|\mathbf{v}_{tot}|$. [8] Cloud approaching (\odot) or receding (\otimes), and moving toward (\downarrow) or away from (\uparrow) disk. [9] Possible association with known HVC complexes. Complexes in square brackets do not have distance constraints. For identification of the HVC complexes, see Kalberla & Haud (2006); Putman et al. (2012).

[1]	[2]	[3]	[4]	[5]	[6]	[7]	[8]	[9]
170	16.8	-25.0	73	138	—	240	$\otimes \uparrow$	GCN
234	24.5	-1.8	321	127	—	324	$\otimes \uparrow$	GCN
238	24.8	8.8	37	152	10.0	24	$\odot \downarrow$	C
924	258.5	-39.1	56	39	21.7	85	$\odot \uparrow$	LA
1093	271.0	10.8	8	50	20.9	72	$\odot \downarrow$	LA
1308	285.0	-16.1	118	68	22.4	2	$\odot \downarrow$	LA
1804	334.8	30.7	20	44	—	234	$\odot \downarrow$	L
48	3.9	-63.7	70	124	—	270	$\otimes \uparrow$	MS?
200	21.2	-61.2	236	24	12.3	59	$\odot \downarrow$	MS?
632	224.1	-17.0	8	139	24.0	81	$\otimes \uparrow$	MS?
648	226.6	-33.4	90	25	7.7	27	$\odot \uparrow$	MS?
1221	279.1	-16.7	211	49	8.4	97	$\odot \downarrow$	LA
1616	316.9	-76.8	94	67	—	166	$\odot \downarrow$	MS
1806	335.0	16.1	191	50	29.4	41	$\odot \uparrow$	[WD]

the results of the method are thus far consistent with existing distance constraints.

The weakest link in these distance constraints is the choice of a halo rotation model. Increasing the characteristic scale from 10 to 20 kpc in equation 5 (and thus flattening the

drop-off of Θ with z) increases all the distance constraints by a factor of ~ 2 . Halo rotation models without z -dependence (Hodges-Kluck et al. 2016) do not yield results if we assume $v_{rel} \lesssim 100 \text{ km s}^{-1}$. We interpret this as a limitation of our assumptions regarding v_{rel} rather than a limitation of the method itself.

4.2 Caveats

Residual Fitting Correcting the inclination angle estimate (equation 3) by fitting the residuals raises the question about the physical motivation for equation 4. Equation 3 assumes that the velocity gradient along the tail, caused by deceleration of the cloud gas, is linear. This is not necessarily correct (Brüns et al. 2001; Peek et al. 2007, see also Fig. 2); material directly behind the cloud is expected to travel nearly at the same velocity as the cloud. Velocities close to the cloud speed reduce the velocity asymmetry a_v , thus overestimating α_i . The fit parameters might also depend on environmental factors, such as the ambient density, and the absolute cloud velocity. These dependencies and their quantification can only be explored with a larger model grid, which is beyond the scope of this paper.

Effect of Background Flow on α_i Since the CHVCs in our sample are identified via HI emission, their α_i estimates rest on the assumption that the neutral gas interacts directly with the background halo. Yet, there is evidence for substantial ionized envelopes co-moving with HVCs (Hill et al. 2009; Lehner et al. 2009, 2012). For a CHVC moving at a velocity $|\mathbf{v}_{tot}| = v_{rel} + v_{env}$ with respect to an ionized envelope traveling in the same direction at v_{env} , the reduced

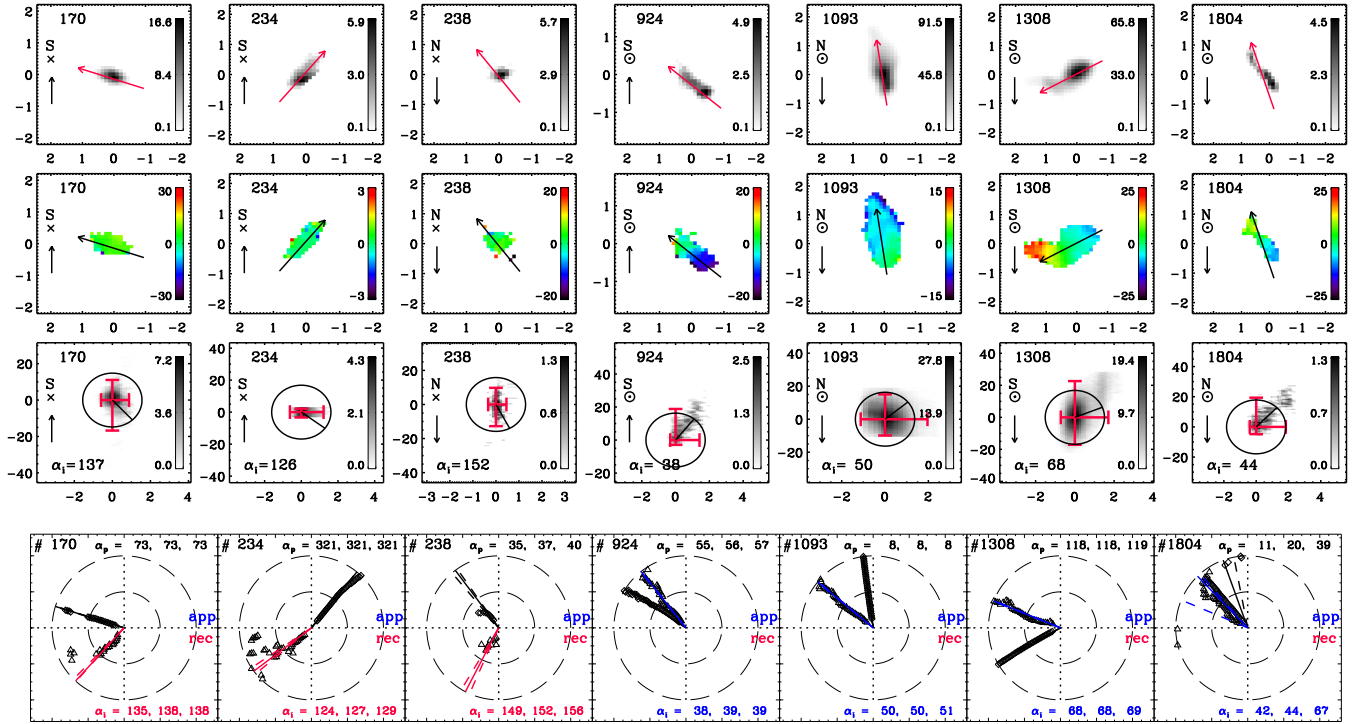


Figure 4. Top to bottom: Integrated intensity for CHVCs selected from HIPASS (Putman et al. 2002), velocity centroid maps, position-velocity plots, and derived position and inclination angles. Red arrows denote the direction of the cloud tail. Positions in (GL, GB) are relative to the cloud’s catalogued coordinates. Letters N and S indicate Northern or Southern Galactic hemisphere. Black vertical arrows indicate whether the cloud is moving toward lower (downward) or higher $|z|$ (upward). Clouds approaching the observer ($\alpha_i < 90^\circ$) are denoted by a dotted circle, otherwise by a “x”. The position axis in the pv-plots is counted from head to tail. *Bottom row:* Position angle α_p (black symbols, lines) and inclination angle α_i (blue or red symbols, lines). Both angles α_p and α_i are counted counter-clockwise from the top, with $0 \leq \alpha_p \leq 360$ and $0 \leq \alpha_i \leq 180$. Long dashed circles indicate S/N values of 20 and 40. Solid lines refer to the median value, short dashed lines to the lower and upper quartile. These values are given also at the top and bottom of each panel (lower quartile, median, upper quartile). The horizontal dashed line separates inclination angles for approaching (blue) and receding (red) CHVCs.

drag results in a smaller spread along the velocity axis in the position-velocity plot, and therefore in a pitch angle biased toward 90° . This in turn increases the inferred total velocity v_{tot} . On the other hand, the observed radial velocity combines the line-of-sight component of the HI CHVC and the ionized envelope. Therefore, our method tends to *overestimate* $|v_{tot}|$ if the CHVC is moving within a larger ionized envelope. Yet, if the line-of-sight component of the envelope’s velocity – and therefore the line-of-sight component of v_{rel} – is known, the velocity spread in the position-velocity plot correctly refers to v_{rel} , and thus α_i is not affected by the ionized envelope.

Effects of Cloud Evolution on α_i The interaction of the CHVC with the ambient gas leads to turbulent structures, and occasionally to large “chunks” of the cloud being ripped off. Such “secular” events can affect the estimates for α_i and α_p . The strong time variations in the residuals of α_i (Fig. 3b,d) are caused by this effect.

The α_i estimate relies on the translation of the effect of the hydrodynamic drag on the CHVC’s tail into centroid velocity profiles. The method assumes a monotonic centroid velocity profile, i.e. for a cloud moving at an angle toward the observer, the head would have the most negative velocities, and the tail the most positive ones. Yet, the centroid velocity map of Fig. 2 demonstrates that this need not be the case (also Brüns et al. 2001). The swath of “green” (less

negative) velocities at the head of the cloud is caused by material flowing around the cloud away from the observer.

5 SUMMARY

We present a method to determine the three-dimensional orientation of CHVCs. The inclination angle is derived from asymmetries in the intensity distribution of a CHVC’s position-velocity plot (Figs. 2 and 4). We test the method with the help of numerical simulations of CHVCs and identify possible systematic effects on the inclination angle estimate. When applied to CHVCs drawn from HIPASS, the method is returning results that are stable with increasing signal-to-noise. The method can be improved by a more detailed analysis of the position-velocity plots, and by a more rigorous statistical treatment. Applications to clouds being ablated in other astrophysical environments seem obvious.

We discuss the possibility to constrain distances by assuming a limiting CHVC velocity with respect to the background medium. Such a limit constrains the possible locations of a CHVC along its line-of-sight, given a Galactic halo rotation model. We find lower distance limits for $\sim 50\%$ of the selected HIPASS CHVC sample. The estimates are consistent with previous distance constraints.

ACKNOWLEDGEMENTS

We thank the referee for a very thorough and concise report. This work was partially supported by UNC Chapel Hill, and it has made use of NASA’s Astrophysics Data System.

REFERENCES

- Benjamin R. A., Danly L., 1997, [ApJ](#), **481**, 764
- Bland-Hawthorn J., Putman M. E., 2001, in Hibbard J. E., Rupen M., van Gorkom J. H., eds, *Astronomical Society of the Pacific Conference Series Vol. 240, Gas and Galaxy Evolution*. p. 369 ([arXiv:astro-ph/0110043](#))
- Brüns C., Kerp J., Kalberla P. M. W., Mebold U., 2000, [A&A](#), **357**, 120
- Brüns C., Kerp J., Pagels A., 2001, [A&A](#), **370**, L26
- Fich M., Blitz L., Stark A. A., 1989, [ApJ](#), **342**, 272
- Fox A. J., et al., 2016, [ApJ](#), **816**, L11
- Heitsch F., Putman M. E., 2009, [ApJ](#), **698**, 1485
- Hill A. S., Haffner L. M., Reynolds R. J., 2009, [ApJ](#), **703**, 1832
- Hodges-Kluck E. J., Miller M. J., Bregman J. N., 2016, [ApJ](#), **822**, 21
- Jin S., 2010, [MNRAS](#), **408**, L85
- Kalberla P. M. W., Haud U., 2006, [A&A](#), **455**, 481
- Lehner N., Staveley-Smith L., Howk J. C., 2009, [ApJ](#), **702**, 940
- Lehner N., Howk J. C., Thom C., Fox A. J., Tumlinson J., Tripp T. M., Meiring J. D., 2012, [MNRAS](#), **424**, 2896
- Levine E. S., Heiles C., Blitz L., 2008, [ApJ](#), **679**, 1288
- Lockman F. J., Benjamin R. A., Heroux A. J., Langston G. I., 2008, [ApJ](#), **679**, L21
- Olano C. A., 2008, [A&A](#), **485**, 457
- Peek J. E. G., Putman M. E., McKee C. F., Heiles C., Stanimirović S., 2007, [ApJ](#), **656**, 907
- Peek J. E. G., Putman M. E., Sommer-Larsen J., 2008, [ApJ](#), **674**, 227
- Putman M. E., et al., 2002, [AJ](#), **123**, 873
- Putman M. E., Bland-Hawthorn J., Veilleux S., Gibson B. K., Freeman K. C., Maloney P. R., 2003, [ApJ](#), **597**, 948
- Putman M. E., Saul D. R., Mets E., 2011, [MNRAS](#), **418**, 1575
- Putman M. E., Peek J. E. G., Jounge M. R., 2012, [ARA&A](#), **50**, 491
- Richter P., de Boer K. S., Werner K., Rauch T., 2015, [A&A](#), **584**, L6
- Saul D. R., et al., 2012, [ApJ](#), **758**, 44
- Stanimirović S., et al., 2006, [ApJ](#), **653**, 1210
- Thom C., Putman M. E., Gibson B. K., Christlieb N., Flynn C., Beers T. C., Wilhelm R., Lee Y. S., 2006, [ApJ](#), **638**, L97
- Thom C., Peek J. E. G., Putman M. E., Heiles C., Peek K. M. G., Wilhelm R., 2008, [ApJ](#), **684**, 364
- Wakker B. P., 2001, [ApJS](#), **136**, 463
- Wakker B. P., van Woerden H., 1997, [ARA&A](#), **35**, 217
- Wakker B. P., et al., 2007, [ApJ](#), **670**, L113

This paper has been typeset from a \LaTeX file prepared by the author.